Geophysical Research Letters

RESEARCH LETTER
10.1029/2024GL108525

Slip-Dependence of Fault Frictional Stability Under Hydrothermal Conditions

Wei Feng[1], Lu Yao[2], Rodrigo Gomila[1], Shengli Ma[2], Giorgio Pennacchioni[1], and Giulio Di Toro[1,3]

[1]Dipartimento di Geoscienze, Università degli Studi di Padova, Padua, Italy, [2]State Key Laboratory of Earthquake Dynamics, Institute of Geology, China Earthquake Administration, Beijing, China, [3]Sezione Roma 1, Istituto Nazionale di Geofisica e Vulcanologia, Rome, Italy

Key Points:

- The role of slip displacement in controlling fault stability under hydrothermal conditions is investigated
- The critical velocity for transition in friction from velocity-weakening to velocity-strengthening increases with slip displacement
- This frictional transition, attributed to chemical alteration, is accompanied by the transition from localized to delocalized deformation

Supporting Information:

Supporting Information may be found in the online version of this article.

Correspondence to:

W. Feng and L. Yao,
wei.feng@unipd.it;
luyao@ies.ac.cn

Citation:

Feng, W., Yao, L., Gomila, R., Ma, S., Pennacchioni, G., & Di Toro, G. (2024). Slip-dependence of fault frictional stability under hydrothermal conditions. *Geophysical Research Letters*, *51*, e2024GL108525. https://doi.org/10.1029/2024GL108525

Received 26 JAN 2024
Accepted 11 JUL 2024

Author Contributions:

Conceptualization: Wei Feng, Lu Yao, Giulio Di Toro
Data curation: Wei Feng, Lu Yao
Funding acquisition: Lu Yao, Shengli Ma, Giorgio Pennacchioni, Giulio Di Toro
Investigation: Wei Feng, Lu Yao, Rodrigo Gomila, Giorgio Pennacchioni
Methodology: Wei Feng, Lu Yao, Giulio Di Toro
Project administration: Shengli Ma, Giulio Di Toro
Supervision: Lu Yao, Giulio Di Toro
Validation: Wei Feng, Lu Yao, Giorgio Pennacchioni, Giulio Di Toro
Visualization: Wei Feng

Abstract In the rate-state friction law framework, the transition from velocity weakening (*V-W*) to velocity strengthening (*V-S*) behavior marks the base of the seismogenic crust. Here we investigate the role of fault slip displacement under hydrothermal conditions in controlling the *V-W* to *V-S* transition. We shear simulated gabbro gouges at slip velocities ranging from 16 nm/s (~50 cm/year) to 10 μm/s (~8 cm/day) under hydrothermal conditions (300–400°C temperature; 30 MPa pore fluid pressure). We observe that cumulative fault slip increases the critical velocity for the *V-W* to *V-S* transition. The transition is accompanied by localized to distributed deformation mode, the formation of smectite-type clays and occurrence of intergranular mass transfer. Our results provide insights into understanding the deepening and shallowing of *V-W*/*V-S* boundary (lower limit of the seismogenic zone) following a mainshock. Besides strain rate effects, slip-enhanced chemical alteration and grain size-sensitive deformation may temporarily contribute to the shallowing process.

Plain Language Summary According to the standard model of earthquake nucleation, earthquakes are the result of frictional instabilities along faults. The necessary condition for earthquake nucleation is that the frictional strength of a fault decreases with fault slip velocity ("velocity-weakening" behavior) or slip distance ("slip-weakening" behavior). Although extensive laboratory studies have been conducted to investigate the velocity-dependence of friction in rocks, less attention was paid to the role of slip displacement on fault frictional stability, especially in the presence of hot and pressurized fluids. The latter, difficult to reproduce in the laboratory, is a common condition at seismogenic depths. In this study, we examine how the frictional stability evolves with slip velocity and displacement on simulated faults made of powders of gabbro (a common rock of the oceanic crust) under hydrothermal conditions up to 400°C. We find that the critical velocity for the transition from velocity-weakening to velocity-strengthening increases with cumulative slip displacement. In nature, the increase of this critical velocity may result in the uplift, during seismic sequences, of the base of the seismogenic crust (i.e., aftershock hypocenters will be shallower). Our findings suggest that, slip displacement, accompanied by fault mineralogical-structural evolution, can influence fault frictional stability and earthquake nucleation.

1. Introduction

In the standard model of earthquake nucleation, the necessary condition is that the fault strength, described by the friction coefficient, decreases with increasing fault slip displacement *d* and slip velocity *V* (slip weakening *S-W* and velocity weakening *V-W* behavior: Dieterich, 1978, 1979; Ruina, 1983; Ohnaka, 2013; Rice, 2006). The dependence of fault friction with *V* is described by the empirical rate and state friction law (RSFL: Dieterich, 1979; Ruina, 1983; Marone, 1998). Because earthquakes in the upper crust nucleate often in the presence of hot and pressurized fluids, a number of experimental studies have been conducted on crustal rocks (e.g., gabbro, granite, limestone, quartz- or phyllosilicate-rich rocks, etc.) under "hydrothermal conditions," indicating that the frictional behavior of faults depends on ambient temperature (Blanpied et al., 1991; den Hartog et al., 2012; Okuda et al., 2023; He et al., 2007; Nakatani & Scholz, 2004). The velocity-stepping (*V*-stepping) experiments (i.e., the slip velocity is increased or decreased abruptly during sliding to measure the response of the dynamic friction coefficient) reveal the presence of three domains of *V*-dependence with increasing temperature (hence, crustal depth). With increasing depth, these include a low temperature velocity-strengthening (*V-S*, friction coefficient increases with increasing *V*) domain, an intermediate temperature *V-W* domain and a high temperature *V-S* domain (Verberne et al., 2015; Chen et al., 2020; Blanpied et al., 1991; He et al., 2007; Zhang & He, 2016; den

Writing – original draft: Wei Feng
Writing – review & editing: Wei Feng, Lu Yao, Rodrigo Gomila, Shengli Ma, Giorgio Pennacchioni, Giulio Di Toro

Hartog et al., 2012; Okuda et al., 2023). The transition from *V-W* to *V-S* frictional behavior at greater depths and temperatures is thought to constrain the lower limit of the seismogenic zone (Scholz, 2019). The *V-W* to *V-S* transition should also roughly overlap to the change in the fault dominant deformation mechanisms (e.g., from cataclasis to dislocation creep) and associated rheology (from elasto-frictional and mainly pressure-dependent to viscous-plastic and mainly temperature-dependent: Handy et al., 2007; Sibson, 1982; Scholz, 2019).

In addition to the temperature-dependence discussed above, the *V-W* to *V-S* transition is also dependent on several other parameters, including pressure, presence of fluids, strain rate, lithology, grain size, etc (Chen et al., 2020; Okuda et al., 2023; Scholz, 2019; Verberne et al., 2015). In particular, because of technical limitations in triaxial machines which limit slip displacement to <1 cm for hydrothermal experiments, the role of slip displacement in the *V-W* to *V-S* transition has not been investigated in depth, although its influence on frictional healing and sliding behavior at room conditions has been recognized (Beeler et al., 1996; Noel et al., 2023, 2024; Richardson & Marone, 1999; Scuderi et al., 2017; Wong et al., 1992). For hydrothermal ring shear experiments where large displacement could be applied (den Hartog et al., 2012; Okuda et al., 2023), the effect of slip displacement on frictional behavior was not discussed. In this study, we investigate whether the cumulative slip displacement affects the frictional stability transition under hydrothermal conditions. On simulated faults made of gabbro gouges we impose *V*-steps from 16 nm/s (~50 cm/year, almost approaching plate tectonic rates) to 10 μm/s (~8 cm/day) for a cumulative slip displacement up to 70 mm, at temperatures T of 300°C and 400°C, pore fluid pressure P_p of 30 MPa and effective normal stresses σ_{eff} of 50 MPa–100 MPa. In the experiments, the transition from possibly unstable (*V-W*) to stable (*V-S*) frictional behavior occurs with increasing fault slip displacement. This is in contrast with the results of experiments performed under room-temperature conditions, according to which as displacements increases the simulated faults become more unstable (Noel et al., 2023). From microstructural observations we infer that the transition from *V-W* to *V-S* is associated with the transition from localized to distributed deformation in the gouge layer (Rutter, 1986), chemical alteration and occurrence of intergranular mass transfer. Our results highlight that fault frictional stability could evolve with shear displacement and slip history.

2. Methods

The rock used in the experiments is the "Jinan dark green" gabbro (China). The rock is crushed in a mill and sieved with a 180-mesh to obtain powders with grain size of less than 88 μm for the experiments. The mineralogical and chemical compositions are determined with X-Ray Powder Diffraction (XRD) and X-Ray Fluorescence (XRF) (Tables S1 and S2 in Supporting Information S1). The gabbro mainly consists of feldspar, pyroxene, olivine, and minor biotite.

Seven experiments are performed with the Low to High-Velocity rotary shear apparatus (LHVR-Beijing) equipped with a new-conceived hydrothermal vessel, installed at the Institute of Geology, China Earthquake Administration in Beijing, China (Feng et al., 2023; Ma et al., 2014) (Figure S1 in Supporting Information S1). Experiments are conducted at constant σ_{eff} of 50 MPa or 100 MPa, P_p of 30 MPa and T of 300°C or 400°C (Table S3 in Supporting Information S1 for full list). In setting up each experiment, about 0.8 g of gouge powder is distributed evenly between two ring-shaped and surface-grooved pistons (22/28 mm in inner/outer diameter), yielding an initial gouge thickness of ~1.5 mm. The samples are confined laterally by inner and outer metal rings (with MoS_2 coating) to avoid extrusion during compaction and shearing.

The whole gouge assembly is then mounted into the vessel. In each experiment, after achieving the desired ambient conditions of σ_{eff}, P_p and T, the initial "*run-in*" stage is imposed at a slip velocity of 10 μm/s for 5 mm or 7 mm of slip displacement (d). Once a stable friction coefficient ($\mu = \tau/\sigma_{eff}$) is achieved, a series of *V*-steps is applied by switching the load-point velocities over 3 orders of magnitude from 16 nm/s to 10 μm/s. The slip displacement between each *V*-step varies from 0.5 to 2 mm, depending on the slip distance required to reach a new steady-state friction value. To study whether the cumulative slip displacement may affect frictional stabilities, two cycles of *V*-stepping tests (i.e., referred to as Cycle 1 and Cycle 2), separated by a slip displacement of 15–50 mm, are conducted. The experiments lasted up to ~20 hr. Three additional experiments (LHV2609, LHV3063 and LHV3081), with only one cycle or with a limited slip displacement, are performed to investigate the microstructural evolution of the gouge layer with slip displacement and its relation to the measured *V*-dependence. In this study, we focus on the friction coefficient *V*-dependence and do not determine the Rate-State-Friction law parameters (i.e., a, b and the critical slip distance D_c) since steady-state conditions are not reached at low slip

10.1029/2024GL108525

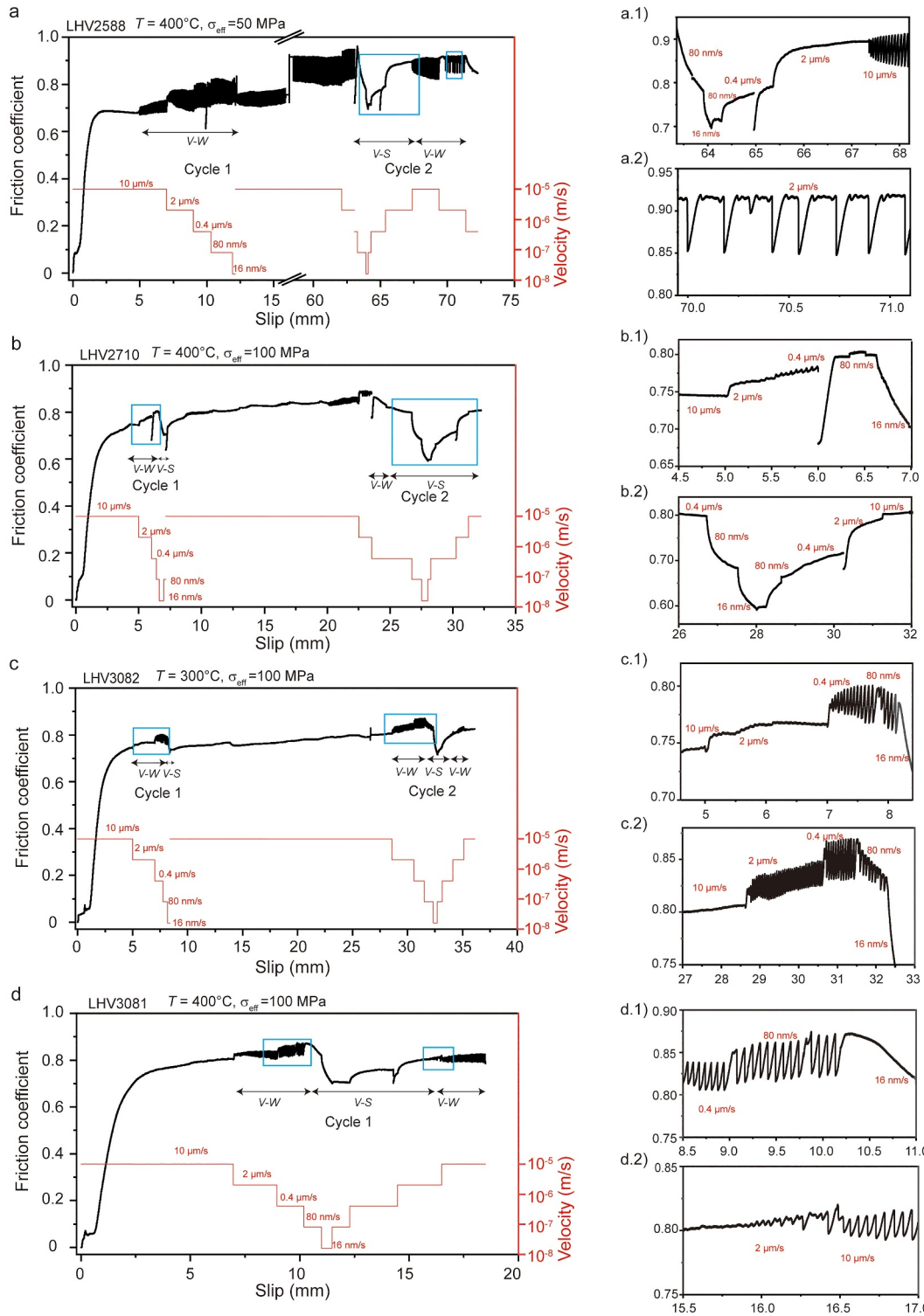

Figure 1. The evolution of the friction coefficient μ versus slip displacement d for the friction experiments of gabbro performed under hydrothermal conditions (temperature T, pore pressure P_p and effective normal stress σ_{eff} are reported in each diagram). Right panel shows close-ups of critical velocity-steps. (a) Experiment LHV2588 performed at $T = 400°C$ and $\sigma_{eff} = 50$ MPa. The emergence of period-multiplying cycle behavior is observed in the transitional regime. (b) Experiment LHV2710 performed at $T = 400°C$ and $\sigma_{eff} = 100$ MPa. (c) Experiment LHV3082 performed at $T = 300°C$ and $\sigma_{eff} = 100$ MPa. (d) Experiment LHV3081 performed at $T = 400°C$ and $\sigma_{eff} = 100$ MPa.

velocities (16–80 nm/s). At the end of the experiment, the deformed samples are recovered for XRD and Scanning Electron Microscope (SEM) investigations. Further details of the experimental setup and methodology can be found in Supporting Information S1 Text S1.

3. Results

3.1. Mechanical Data

The friction coefficient of the sheared gouges and its velocity dependence evolve with slip displacement for all experiments (Figures 1 and 2). In experiment LHV2588 performed at $\sigma_{eff} = 50$ MPa and $T = 400$°C, during the *run-in* at $V = 10$ μm/s, the fault has $\mu_{ss} \sim 0.68$. After $d = 5$ mm, in Cycle 1, a series of *V*-steps are imposed and stick-slip events initiate. In this velocity range (16 nm/s $\leq V \leq$ 10 μm/s) the fault exhibits *V-W* behavior; and the magnitude of the friction coefficient (or stress) drops during stick-slip events increases with decreasing velocity (Figure 1a). After imposing 40 mm of slip displacement at $V = 10$ μm/s (time duration 4,000 s, $d \sim 60$ mm), in Cycle 2, stick-slip and *V-W* behavior are still observed at $2 \leq V \leq 10$ μm/s. However, the stick-slip events vanish and the frictional behavior becomes *V-S* for 16 nm/s $\leq V \leq 2$ μm/s (μ decreases when *V* is decreased from 0.4 μm/s to 16 nm/s and then increases when *V* is increased from 16 nm/s to 2 μm/s, Figure 2). Period-multiplying cycle behavior (i.e., a mixture of stick-slip events characterized by multiple amplitude stress drop, Mei et al., 2021) is observed at this transition *V* of 2 μm/s in the transitional regime (Inset a.2). All these observations are producible in the experiment LHV3080 performed at identical deformation conditions (Figure S2 in Supporting Information S1).

In experiment LHV2710 performed at higher $\sigma_{eff} = 100$ MPa and same $T = 400$°C as LHV2588, in Cycle 1, the fault has a *V-W* behavior for 80 nm/s $\leq V \leq$ 10 μm/s and *V-S* behavior for $16 \leq V \leq 80$ nm/s (Figure 1b). Then, after imposing 15 mm of slip displacement, in Cycle 2, the gouges exhibit stick-slip events and *V-W* behavior for $2 \leq V \leq 10$ μm/s (see $d \sim 23$ mm), and *V-S* behavior for $V < 2$ μm/s. The velocity where the *V-W* to *V-S* transition occurs increases from 80 nm/s (at $d \sim 7$ mm in Cycle 1) to 2 μm/s (at $d \sim 23$ mm in Cycle 2) with increasing slip displacement and shear deformation. Intriguingly, the *V* range for *V-S* behavior is further extended to 10 μm/s at the end of the experiment ($d > 30$ mm) (Figures 1b and 2). In contrast, in experiment LHV3082 performed at $\sigma_{eff} = 100$ MPa but lower $T = 300$°C, in Cycle 1, the fault shows *V-W* behavior for 80 nm/s $\leq V \leq 10$ μm/s and *V-S* behavior for $16 \leq V \leq 80$ nm/s (Figure 1c). After imposing ~15 mm of slip displacement, the velocity for the *V-W* to *V-S* transition increases to 0.4 μm/s in Cycle 2 (at $d \sim 30$ mm), but not as high as that observed at $T = 400$°C.

Summarizing, experimental faults made of gabbro gouges, under the investigated hydrothermal conditions, show transition from *V-W* to *V-S* frictional behavior with decreasing slip velocity. The velocity where this transition occurs is defined as critical slip velocity V_c (red to blue in Figure 2), and V_c increases with cumulative slip displacement. This point is further attested by experiment LHV3081 performed at the same *P-T* conditions of the experiment LHV2710 but without imposing a 15 mm displacement interval (Figure 1d): V_c for *V-S* behavior extends from 0.4 μm/s to 2 μm/s with slip displacement, but lower than V_c of 10 μm/s in experiment LHV2710. This suggests the critical role of slip displacement in controlling instability nucleation, as discussed below.

3.2. Microanalysis of Deformed Samples

3.2.1. Mineral Assemblage

Gabbro-built gouges recovered from experiments that exhibit creep or *V-S* behavior at the end of the slip show a broad peak at $2\theta \sim 8°$ in the XRD spectra, which is absent in the starting materials (Figure 3a). The intensity of the 8° peak increases with temperature (compare LHV3082 performed at 300°C with LHV3080 and LHV3081 performed at 400°C). After separation of the ultra-fine grains, orientation and glycol treatment, this newly formed mineral is identified as smectite-type clay (Brindley & Brown, 1980) (See Figure S3 in Supporting Information S1). In addition, a decrease in the intensity of the biotite peak $2\theta \sim 10°$ is measured in the sheared gouges with respect to the starting materials. XRD data suggests that frictional sliding under the investigated hydrothermal conditions results in the appearance of newly-formed smectite (Na-rich montmorillonite-type mineral).

3.2.2. Microstructures

The microstructures associated with *V-W* and *V-S* friction behavior are investigated by arresting the experiments and recovering the sheared gouge layer at increasing displacement and in different regions.

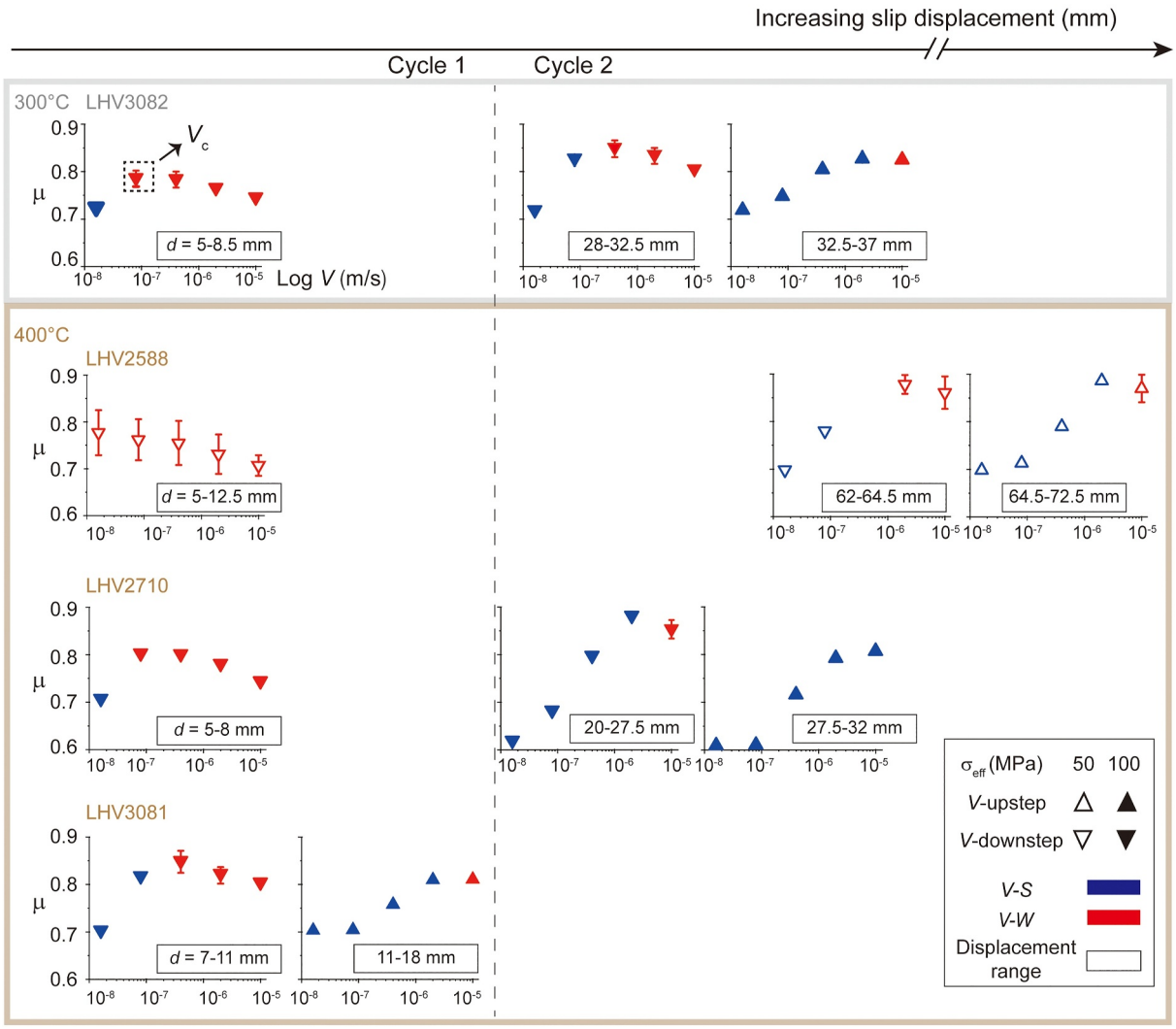

Figure 2. Evolution of the friction coefficient μ and velocity-dependence as a function of slip velocity V for each series of V-steps in the experiments shown in Figure 1. Black numbers in the box indicate the range of slip displacement for individual V-steps Cycle. Symbols in blue and red colors represent V-S and V-W frictional behavior, respectively. The error bars show magnitude of drops in friction coefficient in the stick-slip events.

In experiment LHV3063 (Figure S4 in Supporting Information S1) stopped at d = 9 mm during stick-slip and V-W behavior, strain is localized into ~15 μm-thick slip zone (marked by dashed line in Figure 3b). The slip zone is made of comminuted grains of feldspar and clinopyroxene with sharp edges (Figure 3c). With increasing slip displacement (d = 18 mm, LHV3081), once the gouge layer underwent V-W to V-S and V-S to V-W transitions, the gouge layer is intensely comminuted (Figure S5 in Supporting Information S1). Grain size reduction is larger in the upper ~300–500 μm-thick gouge layers and interpreted as the main slip zone. The slip zone is characterized by intense fragmentation, with sub-angular to rounded grains (<1 μm) and low porosity. Grain size remains as the initial size at the bottom part of the gouges layer. For gouges which underwent an additional 15 mm of slip displacement (LHV2710), after d = 32 mm, deformation is distributed over the entire gouge layer thickness and a S-C fabric, outlined by the spatial arrangement of pyroxene and feldspar grains, is well-developed (Figures 3d and 3e). Grains have sharp edges and angular shapes, indicative of cataclastic flow. The matrix includes up to 1 μm long acicular in shape grains interpreted as newly-formed smectite-type clays (write arrows, Figure 3f). The neck grain boundaries are partly observed (yellow arrows, Figure 3g), suggesting that mass transfer process may take place.

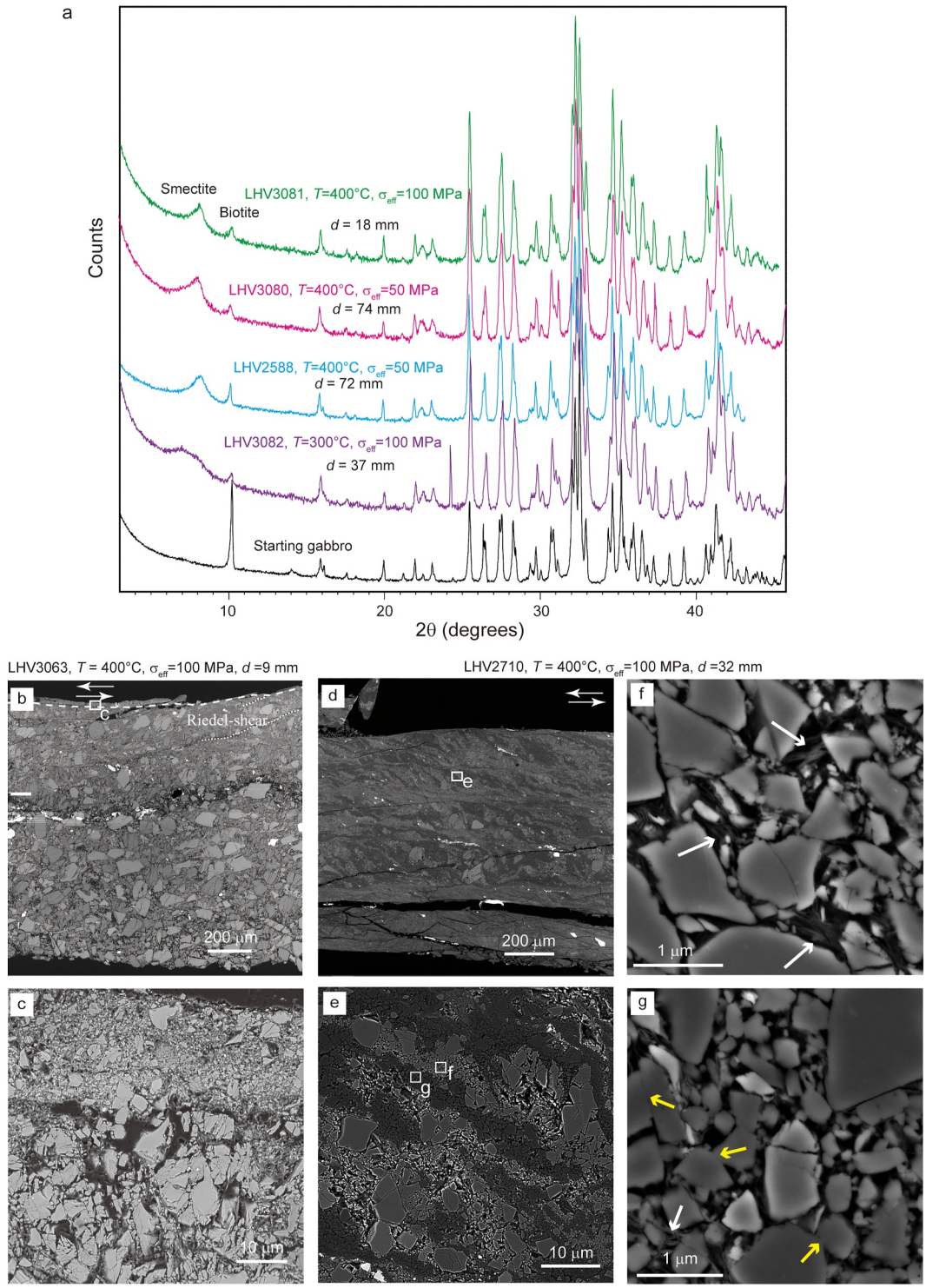

Figure 3. Microanalytical results of deformed gouges recovered from friction experiments. (a) X-ray diffraction (XRD) spectra of representative samples (experimental conditions are reported in each diagram). The appearance of the peak at 2θ ~8° in the sheared gouges is indicative of the presence of newly-formed smectite-type clays. (b–g) Microstructures of sheared gabbro from three experiments at $T = 400$°C and $\sigma_{eff} = 100$ MPa stopped at different displacements. Experimental conditions are reported in the top images. (b–c) LHV3069, $d = 7$ mm d-g. LHV2710, $d = 32$ mm. White arrows indicate the newly-formed clays, yellow arrows point to neck grain boundaries indicative of diffusive mass transfer.

4. Discussion

4.1. Slip-Dependence of the Frictional Behavior

The goal of this study is to explore how frictional stability of gabbro gouges evolves with shear displacement under hydrothermal conditions. The mechanical data shown in Figures 1 and 2 highlight the transition from velocity weakening (possibly resulting in frictionally unstable behavior) to velocity strengthening (frictionally stable) regime with decreasing slip velocity, which can be promoted by increasing slip displacement. The frictional response to *V*-steps in the *V*-*S* regime is gradual (e.g., Figure 1b, b.2) rather than instantaneous as usually observed in the RSF framework (Dieterich, 1979; Marone, 1998). The microstructural analysis of the deformed gouges arrested during the *V*-*W* and *V*-*S* regimes (Figures 3b–3g) indicates that this *V*-*W* to *V*-*S* transition is accompanied by the transition from localized to distributed deformation within the gouge layer (Logan et al., 1992; Logan & Rauenzahn, 1987). However, the deformation mechanism derived from the microstructures remains primarily cataclasis. Because of this, the stability transition may not completely overlap with the brittle-ductile transition usually referred to by geologists.

In general, the transition of frictional stability from *V*-*W* to *V*-*S* has widely been recognized in previous friction experiments performed on calcite, granite, basalt, gabbro, olivine, phyllosilicate-rich mylonite, illite-rich shale by increasing temperature or decreasing slip velocity (Barbot & Zhang, 2023; Blanpied et al., 1991; Chen et al., 2020; den Hartog et al., 2012; He et al., 2007; Okuda et al., 2023; Verberne et al., 2015; Zhang & He, 2016; Zhang et al., 2017). Particularly, this temperature- and velocity-dependent transition in halite and calcite is interpreted by the transition in deformation mechanism from granular sliding to rate- and temperature-dependent creep (Chen & Spiers, 2016; Shimamoto, 1986; Shimamoto & Noda, 2014). Although no evidence of typical crystal plastic deformation in the *V*-*S* regime is captured, we still observe a correlation between temperature and velocity for this stability transition. This is consistent with previous studies that the higher temperature corresponds to a higher V_c. For instance, for basalt gouges, at T = 500–550°C, V_c is 30–100 μm/s, whereas at T = 400–450°C V_c decreases to 3–10 μm/s (Okuda et al., 2023). Our results also suggest that this *V*-*W* to *V*-*S* transition can be promoted by shear displacement, that is, V_c increases with slip (Figure 2), which have not been previously observed. In fact, the effect of shear displacement on fault stability has been systemically investigated at room conditions: Beeler et al. (1996) showed that the velocity dependence of Westerly granite gouge evolves from *V*-*S* to *V*-*W*, then back to *V*-*S* or *V*-neutral with displacement. Noel et al. (2023) showed that the simulated faults of quartz-rich rocks become more unstable with increasing slip displacement. They linked this stability transition to the degree of localized deformation. Also in the experiments presented here but under hydrothermal conditions, the transition from localized to distributed deformation is associated with the transition from *V*-*W* to *V*-*S* behavior. However, in our experiments, the fault slip displacement favors stable sliding rather than frictional instability.

How slip displacement contributes to this stabilization transition under hydrothermal conditions observed here can be attributed to the chemical alteration and diffusive mass transfer. Newly-formed smectites are present in the deformed samples that underwent sufficient long displacement and exhibit frictional *V*-*S* behavior (Figure 3a). Previous experiments indicated that smectite or smectite-rich gouges are characterized, in water-saturated conditions, by a *V*-*S* behavior (Moore & Lockner, 2007; Saffer & Marone, 2003; Tesei et al., 2015). Moreover, grain size reduction due to shear-induced comminution result in an increase in surface area, promoting the activation of hydrothermal alteration process (e.g., the formation of smectite in this study; Callahan et al., 2019) and grain size sensitive deformation (neck grain boundaries; Figure 3g). These effects will be boosted at higher σ_{eff} and higher temperature, which increases the amount of the smectite produced and promotes diffusive mass transfer processes (Figures 3f and 3g). These may explain why the stability transition exhibits a temperature dependence.

However, smectite is thought to be unstable and turn into illite at T > 150°C (Mills et al., 2023). Two questions arise: (a) whether smectite may stably exist at elevated temperatures (e.g., 400°C) during our experiment duration (Derkowski & Kuligiewicz, 2022; Odom, 1984), and (b) if the abundance of smectite is sufficient to control the frictional properties of the fault gouge. Comparison of XRD pattern of pure Na-rich montmorillonite, the same type of smectite formed, and of the ones subjected to uniaxial compaction at 400°C and P_p = 30 MPa for 12 hr shows that they are similar (Figure S6 in Supporting Information S1). We infer that the process of smectite breakdown takes longer time than the duration of our experiments, and that newly formed smectites grow at 400°C and survive during cooling to room temperature. However, considering that smectite is probably metastable under these temperature conditions, at the time scale of seismic cycle, the longevity of these newly-formed

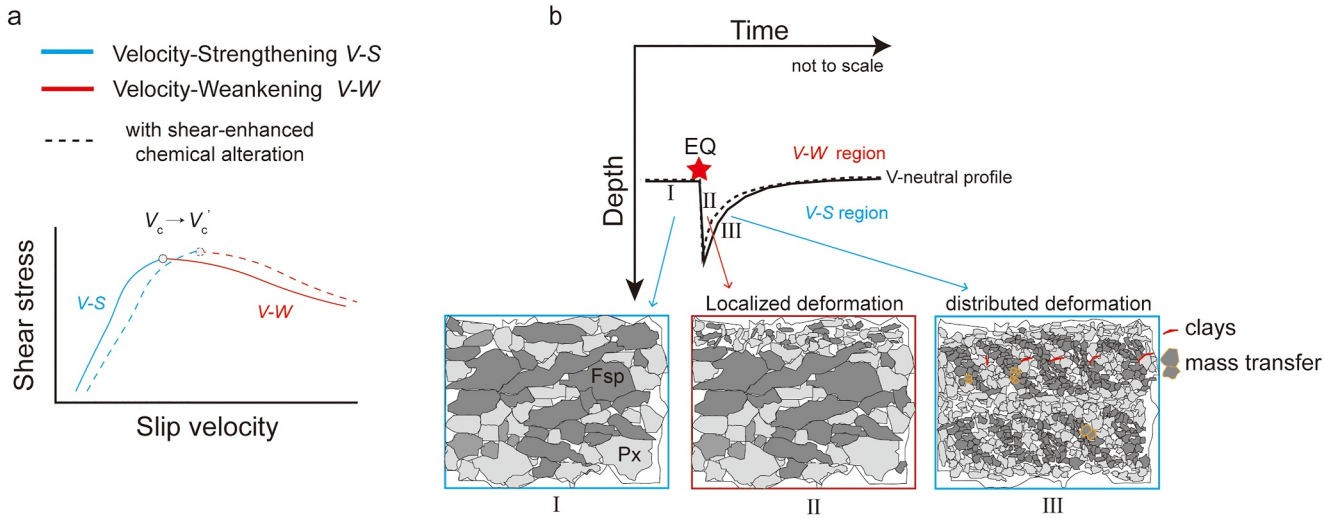

Figure 4. Conceptual diagram of the effect of slip displacement on fault frictional stability. (a) The critical slip velocity (V_c) at which the transition from *V-S* to *V-W* occurs shifts toward higher values with fault slip-enhanced chemical alteration. (b) Depths profile of velocity dependence of fault friction over time near the lower boundary of the seismogenic zone for a simplified seismic cycle. Black lines represent *V*-neutral profile. This boundary deepens and then shallows during the postseismic stage because of the changes in strain rate induced by the mainshock. The faults patches located beneath the seismogenic zone may experience a transition from *V-S* to *V-W* induced by increased slip rate, and back to *V-S* with decreased slip rate (Stages I to III). The latter shallowing process could be promoted by slip-enhanced chemical alteration (dashed line). Fsp = Feldspar; Px = Pyroxene.

clays at seismogenic depths is questioned (Schuck et al., 2018). These smectite-type minerals, which are expected to be concentrated within the slip zone where fluid-rock interaction is more intense due to grain size reduction, can impact the frictional response of gouge layer subjected to shear (Collettini et al., 2009; Niemeijer et al., 2010).

4.2. Geological Implications

Based on the experimental evidence presented, the formation of alteration products and occurrence of grain-size sensitive deformation processes indeed affect the frictional stability of faults: faults become more stable with shear displacement. V_c for the *V-S* to *V-W* transition increases, meaning that faults are stable over a broader range of sub-seismic slip rates (Figure 4a and Figure S7 in Supporting Information S1). As applied to tectonic faults, this stability transition promoted by shear-enhanced chemical alteration may take place locally in the area experiencing intense deformation, for example, the fault patches where coseismic slip occurred. In nature, the hypocentral depth of aftershocks is found to increase immediately after the mainshock and then to decrease gradually with time (Cheng & Ben-Zion, 2019; Rolandone et al., 2004). A plausible explanation is that the so called "brittle-ductile transition" deepens and then shallows during the postseismic stage because of the changes in strain rate in the root of the fault zone (solid line in Figure 4b; e.g., Schaff et al., 2002; Tse & Rice, 1986). In particular, the later relaxation of slip rate shifts the base of the seismogenic zone to a shallower depth (Nishimura & Thatcher, 2003). In addition to changes in slip rate, we suggest that chemical alteration may occur on the newly exposed surfaces, which could be facilitated by grain size reduction during coseismic slip and early afterslip. As a consequence, the stabilization effect due to chemical alteration may temporarily and locally play a role by increasing V_c, contributing to the shallowing of *V-S* to *V-W* transition (black dashed line in Figure 4b). Based on experimental observations, we propose that faults patches located beneath the seismogenic zone may undergo, after a mainshock, a transition from *V-S* to *V-W* induced by the stress perturbations, and back to *V-S* that can be promoted by chemical alteration (Stages I to III).

Although in this study we attempt to investigate the impact of slip displacement on fault friction under hydrothermal conditions, a common condition in Earth's seismogenic crust, the study suffers from several limitations. For example, we employed only gabbro and studied its interaction with distilled water. It is well known that natural fluids can have wide compositional variations that affect the type of newly formed minerals, ranging from clays ("soft" and *V-S*) to quartz and epidote ("hard" and *V-W*) (e.g., Di Toro & Pennacchioni, 2005; Wintsch et al., 1995). Furthermore, given the experimental setup, we could not consider the geometric complexity of fault zones, including the variable thickness of fault slip zones, the roughness of fault surfaces, and, on a larger scale,

the network of minor and major faults/fractures and the presence of damage zones (Faulkner et al., 2010; Wibberley et al., 2008). All these geometric parameters contribute to the evolution in space and time of the velocity dependence of the so-called "coefficient of friction." Moreover, although our experiments lasted up to 20 hr, fluid-rock interaction during the afterslip takes months to years, and we could only partially address the role of time.

5. Conclusions

Our study highlights that slip displacement-enhanced chemical alteration in the presence of hot and pressurized water affects the frictional behavior of faults, contributing to the transition from *V-W* to *V-S* behavior at higher V_c (Figures 1 and 2). This transition in frictional behavior is controlled by cataclastic processes, and by the appearance of newly formed clays and intergranular mass transfer. The transition is also associated with the transition from localized to distributed deformation. In a seismic sequence, the shift of the frictional transition to higher V_c temporarily contributes, together with the post-mainshock relaxation, to the rise of the base of the seismogenic zone.

Data Availability Statement

All datasets collected in this study are available at Feng et al. (2024).

Acknowledgments
This research was supported by the National Natural Science Foundation of China Grants 42174223, 41774191 and 42111530030 to L.Y. and Grant U1839211 to S.M., CSC No. 201906440130 to W.F., the ERC CoG project NOFEAR 614705, MUR and Italian Civil Protection projects PRIN 2022WE2JY9 and EXTEND to G.D. T., PRIN 2020WPMFE9 "THALES" to G. P., and MSCA No. 896346 FRICTION to R.G. We thank Marco Favero and Xi Ma (XRPD), Daria Pasqual (XRF), Leonardo Tauro (sample preparation), and Jacopo Nava (FEG-SEM) for technical support. Chris Spiers is thanked for insightful discussions. We thank the editor Germán Prieto, the associate editor and two anonymous reviewers for their constructive comments that greatly helped us to improve the quality of the manuscript. Open access publishing facilitated by Universita degli Studi di Padova, as part of the Wiley - CRUI-CARE agreement.

References

Barbot, S., & Zhang, Z. (2023). Constitutive behavior of olivine gouge across the brittle-ductile transition. *Geophysical Research Letters*, *50*(24), e2023GL105916. https://doi.org/10.1029/2023GL105916

Beeler, N. M., Tullis, T. E., Blanpied, M. L., & Weeks, J. D. (1996). Frictional behavior of large displacement experimental faults. *Journal of Geophysical Research*, *101*(B4), 8697–8715. https://doi.org/10.1029/96JB00411

Blanpied, M. L., Lockner, D. A., & Byerlee, J. D. (1991). Fault stability inferred from granite sliding experiments at hydrothermal conditions. *Geophysical Research Letters*, *18*(4), 609–612. https://doi.org/10.1029/91GL00469

Brindley, G., & Brown, G. (1980). *Crystal structures of clay minerals and their X-ray identification*. Mineralogical Society of Great Britain and Ireland.

Callahan, O. A., Eichhubl, P., Olson, J. E., & Davatzes, N. C. (2019). Fracture mechanical properties of damaged and hydrothermally altered rocks, Dixie valley-Stillwater fault zone, Nevada, USA. *Journal of Geophysical Research: Solid Earth*, *124*(4), 4069–4090. https://doi.org/10.1029/2018JB016708

Chen, J., & Spiers, C. J. (2016). Rate and state frictional and healing behavior of carbonate fault gouge explained using microphysical model. *Journal of Geophysical Research: Solid Earth*, *121*(12), 8642–8665. https://doi.org/10.1002/2016JB013470

Chen, J., Verberne, B. A., & Niemeijer, A. R. (2020). Flow-to-friction transition in simulated calcite gouge. Experiments and microphysical modeling. *Journal of Geophysical Research: Solid Earth*, *12*(11), e2020JB019970. https://doi.org/10.1029/2020JB019970

Cheng, Y., & Ben-Zion, Y. (2019). Transient brittle-ductile transition depth induced by moderate-large earthquakes in Southern and Baja California. *Geophysical Research Letters*, *46*(20), 11109–11117. https://doi.org/10.1029/2019GL084315

Collettini, C., Niemeijer, A., Viti, C., & Marone, C. (2009). Fault zone fabric and fault weakness. *Nature*, *462*(7275), 907–910. https://doi.org/10.1038/nature08585

den Hartog, S. A. M., Niemeijer, A. R., & Spiers, C. J. (2012). New constraints on megathrust slip stability under subduction zone P–T conditions. *Earth and Planetary Science Letters*, *353–354*, 240–252. https://doi.org/10.1016/j.epsl.2012.08.022

Derkowski, A., & Kuligiewicz, A. M. (2022). Thermal analysis and thermal reactions of smectites: A review of methodology, mechanisms, and kinetics. *Clays and Clay Minerals*, *70*(6), 946–972. https://doi.org/10.1007/s42860-023-00222-y

Dieterich, J. H. (1978). Time-dependent friction and the mechanics of stick-slip. *Pure and Applied Geophysics*, *116*(4–5), 790–806. https://doi.org/10.1007/BF00876539

Dieterich, J. H. (1979). Modeling of rock friction: 1. Experimental results and constitutive equations. *Journal of Geophysical Research*, *84*(B5), 2161–2168. https://doi.org/10.1029/JB084iB05p02161

Di Toro, G., & Pennacchioni, G. (2005). Fault plane process and mesoscopic structure of a strong-type seismogenic fault in tonalites (Adamello batholith, Southern Alps). *Tectonophysics*, *402*(1–4), 55–80. https://doi.org/10.1016/j.tecto.2004.12.036

Faulkner, D. R., Jackson, C. A. J., Lunn, R. J., Schlische, R. W., Shipton, Z. K., Wibberley, C. A. J., & Withjack, M. O. (2010). A review of recent developments concerning the structure, mechanics and fluid flow properties of fault zones. *Journal of Structural Geology*, *32*(11), 1557–1575. https://doi.org/10.1016/j.jsg.2010.06.009

Feng, W., Yao, L., Cornelio, C., Gomila, R., Ma, S., Yang, C., et al. (2023). Physical state of water controls friction of gabbro-built faults. *Nature Communications*, *14*(1), 4612. https://doi.org/10.1038/s41467-023-40313-x

Feng, W., Yao, L., Ma, S., & Di Toro, G. (2024). Slip-dependence of fault frictional stability under hydrothermal conditions [Dataset]. *Zenodo*. https://doi.org/10.5281/zenodo.10491448

Handy, M., Hirth, G., & Hovius, N. (2007). *Tectonic faults*. MIT Press.

He, C., Wang, Z., & Yao, W. (2007). Frictional sliding of gabbro gouge under hydrothermal conditions. *Tectonophysics*, *445*(3–4), 353–362. https://doi.org/10.1016/j.tecto.2007.09.008

Logan, J. M., Dengo, C. A., Higgs, N. G., & Wang, Z. Z. (1992). Fabrics of experimental fault zones: Their development and relationship to mechanical behavior. *International Geophysics*, *51*, 33–67. https://doi.org/10.1016/S0074-6142(08)62814-4

Logan, J. M., & Rauenzahn, K. A. (1987). Frictional dependence of gouge mixtures of quartz and montmorillonite on velocity, composition and fabric. *Tectonophysics*, *144*(1–3), 87–108. https://doi.org/10.1016/0040-1951(87)90010-2

Ma, S., Shimamoto, T., Yao, L., Togo, T., & Kitajima, H. (2014). A rotary-shear low to high-velocity friction apparatus in Beijing to study rock friction at plate to seismic slip rates. *Earthquake Science*, *27*(5), 469–497. https://doi.org/10.1007/s11589-014-0097-5

Marone, C. (1998). Laboratory-derived friction laws and their application to seismic faulting. *Annual Review of Earth and Planetary Sciences*, *26*(1), 643–696. https://doi.org/10.1146/annurev.earth.26.1.643

Mei, C., Barbot, S., & Wu, W. (2021). Period-multiplying cycles at the transition between stick-slip and stable sliding and implications for the Parkfield period-doubling tremors. *Geophysical Research Letters*, *48*(7), e2020GL091807. https://doi.org/10.1029/2020GL091807

Mills, M. M., Sanchez, A. C., Boisvert, L., Payne, C. B., Ho, T. A., & Wang, Y. (2023). Understanding smectite to illite transformation at elevated (>100°C) temperature: Effects of liquid/solid ratio, interlayer cation, solution chemistry and reaction time. *Chemical Geology*, *615*, 121214. https://doi.org/10.1016/j.chemgeo.2022.121214

Moore, D. E., & Lockner, D. A. (2007). *Friction of the smectite clay montmorillonite: A review and interpretation of data* (pp. 317–345). Columbia University Press. https://doi.org/10.7312/dixo13866-011

Nakatani, M., & Scholz, C. H. (2004). Frictional healing of quartz gouge under hydrothermal conditions: 1. Experimental evidence for solution transfer healing mechanism. *Journal of Geophysical Research*, *109*(B7), B07201. https://doi.org/10.1029/2001JB001522

Niemeijer, A., Marone, C., & Elsworth, D. (2010). Fabric induced weakness of tectonic faults. *Geophysical Research Letters*, *37*(3), L03304. https://doi.org/10.1029/2009GL041689

Nishimura, T., & Thatcher, W. (2003). Rheology of the lithosphere inferred from postseismic uplift following the 1959 Hebgen Lake earthquake. *Journal of Geophysical Research*, *108*(B8), B82389. https://doi.org/10.1029/2002JB002191

Noel, C., Giorgetti, C., Collettini, C., & Marone, C. (2024). The effect of shear strain and shear localization on fault healing. *Geophysical Journal International*, *236*(3), 1206–1215. https://doi.org/10.1093/gji/ggad486

Noel, C., Giorgetti, C., Scuderi, M. M., Collettini, C., & Marone, C. (2023). The effect of shear displacement and wear on fault stability: Laboratory constraints. *Journal of Geophysical Research: Solid Earth*, *128*(4), e2022JB026191. https://doi.org/10.1029/2022JB026191

Odom, I. E. (1984). Smectite clay minerals: Properties and uses. *Philosophical Transactions of the Royal Society A*, *311*(1517), 391–409. https://doi.org/10.1098/rsta.1984.0036

Ohnaka, M. (2013). *The physics of rock failure and earthquakes*. Cambridge University Press. https://doi.org/10.1017/CBO9781139342865

Okuda, H., Niemeijer, A. R., Takahashi, M., Yamaguchi, A., & Spiers, C. J. (2023). Hydrothermal friction experiments on simulated basaltic fault gouge and implications for megathrust earthquakes. *Journal of Geophysical Research: Solid Earth*, *128*(1), e2022JB025072. https://doi.org/10.1029/2022JB025072

Rice, J. R. (2006). Heating and weakening of faults during earthquake slip. *Journal of Geophysical Research*, *111*(B5). https://doi.org/10.1029/2005JB004006

Richardson, E., & Marone, C. (1999). Effects of normal stress vibrations on frictional healing. *Journal of Geophysical Research*, *104*(B12), 28859–28878. https://doi.org/10.1029/1999JB900320

Rolandone, F., Bürgmann, R., & Nadeau, R. M. (2004). The evolution of the seismic-aseismic transition during the earthquake cycle: Constraints from the time-dependent depth distribution of aftershocks. *Geophysical Research Letters*, *31*(23), L23610. https://doi.org/10.1029/2004GL021379

Ruina, A. (1983). Slip instability and state variable friction laws. *Journal of Geophysical Research*, *88*(B12), 10359–10370. https://doi.org/10.1029/JB088iB12p10359

Rutter, E. H. (1986). On the nomenclature of mode of failure transitions in rocks. *Tectonophysics*, *122*(3–4), 381–387. https://doi.org/10.1016/0040-1951(86)90153-8

Saffer, D. M., & Marone, C. (2003). Comparison of smectite- and illite-rich gouge frictional properties: Application to the updip limit of the seismogenic zone along subduction megathrusts. *Earth and Planetary Science Letters*, *215*(1–2), 219–235. https://doi.org/10.1016/S0012-821X(03)00424-2

Schaff, D. P., Bokelmann, G. H. R., Beroza, G. C., Waldhauser, F., & Ellsworth, W. L. (2002). High-resolution image of calaveras fault seismicity. *Journal of Geophysical Research*, *107*(B9), ESE5-1–ESE5-16. https://doi.org/10.1029/2001JB000633

Scholz, C. H. (2019). *The mechanics of earthquakes and faulting*. Cambridge University Press.

Schuck, B., Janssen, C., Schleicher, A. M., Toy, V. G., & Dresen, G. (2018). Microstructures imply cataclasis and authigenic mineral formation control geomechanical properties of New Zealand's Alpine Fault. *Journal of Structural Geology*, *110*, 172–186. https://doi.org/10.1016/j.jsg.2018.03.001

Scuderi, M. M., Collettini, C., Viti, C., Tinti, E., & Marone, C. (2017). Evolution of shear fabric in granular fault gouge from stable sliding to stick slip and implications for fault slip mode. *Geology*, *45*(8), 731–734. https://doi.org/10.1130/G39033.1

Shimamoto, T. (1986). Transition between frictional slip and ductile flow for halite shear zones at room temperature. *Science*, *23*(4739), 711–714. https://doi.org/10.1126/science.231.4739.711

Shimamoto, T., & Noda, H. (2014). A friction to flow constitutive law and its application to a 2-D modeling of earthquakes. *Journal of Geophysical Research: Solid Earth*, *119*(11), 8089–8106. https://doi.org/10.1002/2014JB011170

Sibson, R. H. (1982). Fault zone models, heat flow, and the depth distribution of earthquakes in the continental crust of the United States. *Bulletin of the Seismological Society of America*, *72*, 151–163. https://doi.org/10.1785/BSSA0720010151

Tesei, T., Lacroix, B., & Collettini, C. (2015). Fault strength in thin-skinned tectonic wedges across the smectite-illite transition: Constraints from friction experiments and critical tapers. *Geology*, *43*(10), 923–926. https://doi.org/10.1130/G36978.1

Tse, S. T., & Rice, J. R. (1986). Crustal earthquake instability in relation to the depth variation of frictional slip properties. *Journal of Geophysical Research*, *91*(B9), 9452–9472. https://doi.org/10.1029/JB091iB09p09452

Verberne, B. A., Niemeijer, A. R., De Bresser, J. H. P., & Spiers, C. J. (2015). Mechanical behavior and microstructure of simulated calcite fault gouge sheared at 20–600°C: Implications for natural faults in limestones. *Journal of Geophysical Research: Solid Earth*, *120*(12), 8169–8196. https://doi.org/10.1002/2015JB012292

Wibberley, C. A. J., Yielding, G., & Di Toro, G. (2008). Recent advances in the understanding of fault zone internal structure: A review. *Geological Society, London, Special Publications*, *299*(1), 5–33. https://doi.org/10.1144/sp299.2

Wintsch, R. P., Christoffersen, R., & Kronenberg, A. K. (1995). Fluid-rock reaction weakening of fault zones. *Journal of Geophysical Research*, *100*(B7), 13021–13032. https://doi.org/10.1029/94JB02622

Wong, T., Gu, Y., Yanagidani, T., & Zhao, Y. (1992). Stabilization of faulting by cumulative slip. *Fault mechanics and transport properties of rocks*, 119–143. https://doi.org/10.1016/S0074-6142(08)62820-X

Zhang, L., & He, C. (2016). Frictional properties of phyllosilicate-rich mylonite and conditions for the brittle-ductile transition. *Journal of Geophysical Research: Solid Earth*, *121*(4), 3017–3047. https://doi.org/10.1002/2015JB012489

Zhang, L., He, C., Liu, Y., & Lin, J. (2017). Frictional properties of the South China Sea oceanic basalt and implications for strength of the Manila subduction seismogenic zone. *Marine Geology*, *394*, 16–29. https://doi.org/10.1016/j.margeo.2017.05.006